Electron-impact ionization of Be-like ions

J.-C. Chang,[1,*] H.-L. Sun,[2] W.-Y. Cheng,[2] and K.-N. Huang[2,3]
[1]*Department of Science Education, National Hsinchu Teachers College, Hsinchu, Taiwan 300, Republic of China*
[2]*Department of Physics, National Taiwan University, Taipei, Taiwan 106, Republic of China*
[3]*Institute of Atomic and Molecular Sciences, Academia Sinica, P. O. Box 23-166, Taipei, Taiwan 106, Republic of China*
(Received 29 September 2003; published 19 May 2004)

Electron-impact ionization cross sections of Be-like ions are studied in the two-potential distorted-wave approximation. The relativistic and nonrelativistic total cross sections for incident energies from 1 to 10 units of ionization energy are calculated for B^+, C^{2+}, N^{3+}, O^{4+}, F^{5+}, Ne^{6+}, Al^{9+}, Ar^{14+}, Fe^{22+}, Ag^{43+}, and Hg^{76+}. Systematic behaviors along the Be isoelectronic sequence are demonstrated.

DOI: 10.1103/PhysRevA.69.052713 PACS number(s): 34.80.Dp, 34.80.Kw

I. INTRODUCTION

Electron-impact ionization processes of atoms and ions are fundamental to almost all types of gas discharges. Specifically, accurate ionization cross sections of highly charged ions are required for diagnostics and impurity radiation studies of fusion reactor processes. However, the difficulties inherent in measuring ionization cross sections of highly charged ions prohibit experimentalists from obtaining extensive data. A study of systematic behaviors of ionization cross sections along isoelectronic sequences provides a solution to this problem.

Electron-impact ionization cross sections of Be-like ions, specifically, B^+, C^{2+}, N^{3+}, and O^{4+}, have been measured by Falk *et al.* [1], C^{2+} by Woodruff *et al.* [2], O^{4+} by Loch *et al.* [3], and Ne^{6+} by Duponchelle *et al.* [4] with the crossed-beam technique, and C^{2+} by Hamdan *et al.* [5] with the trapped-ion-beam technique. Theoretical cross sections of N^{3+}, O^{4+}, and F^{5+} have been reported by Younger [6] with parametrized distorted waves, C^{2+}, N^{3+}, O^{4+}, Ne^{6+}, and Fe^{22+} by Jakubowicz and Moores [7] and O^{4+} by Loch *et al.* [3] using close-coupling wave functions, and Ne^{6+} by Laghdas *et al.* [8] in the distorted-wave Born approximation.

In this work, ionization cross sections of B^+, C^{2+}, N^{3+}, O^{4+}, F^{5+}, Ne^{6+}, Al^{9+}, Ar^{14+}, Fe^{22+}, Ag^{43+}, and Hg^{76+} are calculated in the two-potential distorted-wave (TPDW) approach with exact exchange effects. The TPDW has been applied to impact ionization of hydrogen-, helium-, lithium-, and beryllium-like ions [9–15], for which universal curves of the scaled cross sections have been studied. Threshold behaviors have also been investigated for the electron-impact ionization of H by Chang *et al.* [13] and for the positron-impact ionization of He by Kuo *et al.* [16]. Here, we shall formally report the TPDW results for Be-like ions.

A review of the general theory is given in Sec. II. Numerical results and discussions are provided in Secs. III and IV.

II. THEORY

A. Cross sections of electron-impact ionization

In electron-impact ionization processes, the target ion is ionized by an incident electron of linear momentum $\mathbf{k}_i$ and energy E_i, and the two emerging electrons are described by $(\mathbf{k}_p, E_p)$ and $(\mathbf{k}_s, E_s)$, where the primary (or the faster) electron is specified by subscript p, and the secondary (or the slower) electron by subscript s. By energy conservation, we have

$$E_i + E_b = E_p + E_s, \tag{1}$$

where E_b is the energy of the bound electron.

If both the incident electron and the target ion are unpolarized, the triple-differential cross section in a relativistic formulation have been given by Huang [17] in atomic units as

$$\frac{d^3\sigma}{dE_s d\Omega_p d\Omega_s} = \frac{(2\pi)^4}{c^6}\left[\frac{k_p E_p k_s E_s E_i}{k_i}\right]\sum_{(fi)} |T_{fi}|^2, \tag{2}$$

where c is the speed of light, T_{fi} is the appropriate transition amplitude, and the summation over (fi) denotes symbolically averaging over the initial polarizations and summing over the final polarizations. The single-differential cross section is obtained by integrating over Ω_p and Ω_s as

$$\frac{d\sigma}{dE_s} = \frac{(2\pi)^4}{c^6}\left[\frac{k_p E_p k_s E_s E_i}{k_i}\right]\int d\Omega_p \int d\Omega_s \sum_{(fi)} |T_{fi}|^2 = \frac{2\pi^3}{k_i^2(2J_0+1)}\sum_\alpha d_\alpha^2, \tag{3}$$

where J_0 is the total angular momentum of the target, and the summation is over all possible channels denoted by the index $\alpha \equiv (\kappa_i, \kappa_p, \kappa_s, j, J)$. Here the real amplitude d_α is defined by the reduced matrix element of the partial-wave amplitude in channel α,

$$d_\alpha \exp(i\delta_\alpha) = i^{l_i-(l_p+l_s)}\exp[i(\delta_{\kappa_p}+\delta_{\kappa_s})] \times \langle \alpha^-[J_\alpha(j_p j_s)j]J\|H_I\|(J_0 j_i)J\rangle, \tag{4}$$

where δ_{κ_p} and δ_{κ_s} denote the Coulomb phase shifts of the two outgoing electrons, J_α and J the total angular momentum of the residual ion and of the entire collision complex, and H_I the appropriate interaction Hamiltonian.

The total cross section is obtained by integrating over E_s as

*Electronic address: jcchang@nhctc.edu.tw

$$\sigma = \int_{c^2}^{(E_i+E_b)/2} \frac{d\sigma}{dE_s} dE_s, \tag{5}$$

where c^2 represents the rest energy of the electron.

B. Transition amplitude

For electron-impact ionization of Be-like ions, the total Hamiltonian of the collision system is assumed to be

$$H = \sum_{i=1}^{5} (c\alpha_i \cdot \mathbf{p}_i + c^2\beta_i) - \sum_{i=1}^{5} \frac{Z}{r_i} + \sum_{i<j}^{5} \frac{1}{r_{ij}}, \tag{6}$$

where α_i and β_i are Dirac matrices. Before the collision, the total Hamiltonian H can be decomposed into the unperturbed Hamiltonian H_i and the interaction potential V_i as

$$H_i = (c\alpha_1 \cdot \mathbf{p}_1 + c^2\beta_1) + H_0, \tag{7}$$

$$V_i = -\frac{Z}{r_1} + \sum_{i=2}^{5} \frac{1}{r_{1i}}. \tag{8}$$

where the subscript "1" is the index for the incident electron, H_0 denotes the total Hamiltonian of the target ion with four bound electrons, and V_i represents the interaction potential between the incident electron and the target ion. The transition amplitude may be written in the prior form as

$$T_{fi} = \langle \Psi_f^{(-)} | V_i | \Phi_i \rangle. \tag{9}$$

where Φ_i denotes an eigenfunction of H_i, and $\Psi_f^{(-)}$ an eigenfunction of H with the incoming-wave boundary condition.

C. Two-potential distorted-wave formulation

In the two-potential distorted-wave formulation [13], the potential V_i is split into the distorting potential U_i and residual potential W_i as

$$U_i = -\frac{Z}{r_1} + v_i(r_1), \tag{10}$$

$$W_i = \sum_{i=2}^{5} \frac{1}{r_{1i}} - v_i(r_1), \tag{11}$$

where the effective potential $v_i(r_1)$ may be arbitrary. After some algebra, the transition amplitude in Eq. (9) can be reduced exactly to the form

$$T_{fi} = \langle \Psi_f^{(-)} | W_i | \psi_i^{(+)} \rangle, \tag{12}$$

where the wave function $\psi_i^{(+)}$ is an eigenfunction of $H_i + U_i$ with the outgoing-wave boundary condition. The transition amplitude is independent of the choice of the distorting potential U_i if the eigenfunctions $\Psi_f^{(-)}$ and $\psi_i^{(+)}$ were obtained exactly. Because of the intrinsic difficulties in calculating exact eigenfunctions for many-particle systems, a reasonable distorting potential U_i should be chosen to make the perturbative effects of W_i as small as possible.

D. Antisymmetrization of the transition amplitude

A general procedure of treating exchange effects in scattering processes is followed to antisymmetrize the transition amplitude, instead of the wave functions only. For a Be-like target in its ground state with configuration ($1s^2 2s^2$), we start from the semisymmetrized wave functions $\phi_i^{(+)}$ and $\phi_f^{(-)}$ for the initial and final states, respectively,

$$|\phi_i^{(+)}\rangle = |\chi_i^{(+)}(\mathbf{r}_1)\varphi_{2s}(\mathbf{r}_2,\mathbf{r}_3)\varphi_{1s}(\mathbf{r}_4,\mathbf{r}_5)\rangle, \tag{13}$$

$$|\phi_f^{(-)}\rangle = |\chi_p^{(-)}(\mathbf{r}_1)\chi_s^{(-)}(\mathbf{r}_2)\varphi'_{2s}(\mathbf{r}_3)\varphi'_{1s}(\mathbf{r}_4,\mathbf{r}_5)\rangle, \tag{14}$$

where φ_{1s}, φ_{2s}, and φ'_{1s} are the antisymmetrized subshell wave functions solved from relativistic equations, and $\chi_i^{(+)}$, $\chi_p^{(-)}$, and $\chi_s^{(-)}$ are the relativistic distorted waves to be given in Sec. II E. The matrix element T_{fi} in Eq. (12) after antisymmetrization are then expressed explicitly as

$$T_{fi} = D_{fi} + I_{fi} + C_{fi}, \tag{15}$$

$$D_{fi} = \sqrt{2}\langle (1 - 2Q_{24} - 2Q_{35} + Q_{24}Q_{35})\phi_f^{(-)} | W_i | \phi_i^{(+)} \rangle, \tag{16}$$

$$I_{fi} = -\langle Q_{12}(1 - 2Q_{24} - 2Q_{35} + Q_{24}Q_{35})\phi_f^{(-)} | W_i | \phi_i^{(+)} \rangle, \tag{17}$$

$$\begin{aligned} C_{fi} = &-\langle Q_{13}(1 - 2Q_{24} - 2Q_{35} + Q_{24}Q_{35})\phi_f^{(-)} | W_i | \phi_i^{(+)} \rangle \\ &- 2\langle Q_{14}(1 - Q_{23} - Q_{24} - Q_{34} - Q_{35} + Q_{24}Q_{35})\phi_f^{(-)} \\ &\times | W_i | \phi_i^{(+)} \rangle, \end{aligned} \tag{18}$$

where Q_{ij} denotes the permutation of particle indices i and j. Here we classify contributions in the antisymmetrized transition amplitude in Eq. (15) into three types: the direct, interchange, and capture terms. The direct term D_{fi} in Eq. (16) corresponds to the processes in which the incident electron is scattered and carries more energy than the ejected electron. The interchange term I_{fi} in Eq. (17) corresponds to the direct term with the indices of the two emerging electrons interchanged, in which the scattered electron carries less kinetic energy than the ejected electron. The capture term C_{fi} in Eq. (18) indicates the possible processes in which the incident electron is captured into the $2s$ or $1s$ bound orbitals with two of the initially bounded electrons ejected. We note that exchange effects due to antisymmetrization are not dealt exactly in previous works [6,7].

E. Distorted waves

The initial-state wave function $\psi_i^{(+)}$ is approximated by $\phi_i^{(+)}$ in Eq. (13), where the distorted wave $\chi_i^{(+)}(\mathbf{r}_1)$ is solved from the equation with distorting potential U_i,

$$[c\alpha_1 \cdot \mathbf{p}_1 + c^2\beta_1 + U_i - E_i]\chi_i^{(+)}(\mathbf{r}_1) = 0. \tag{19}$$

Here the effective potential $v_i(r_1)$ in U_i is taken to be the average potential due to the initially bound electrons,

TABLE I. Distorting potentials and asymptotic charges for the primary and secondary electrons in the models used in the calculation, where v_{1s} and v_{2s} denote the average screening due to the ground-state electrons of Be-like ions in the 1*s* and 2*s* orbitals, respectively.

Model	Distorting potential		Asymptotic charges	
	U_p	U_s	Z_p	Z_s
TPDW01	$-z/r_1+v_i(r_1)$	$-Z/r_2+v_f(r_2)$	$(Z-4)$	$(Z-3)$
TPDW11	$-Z/r_1+v_f(r_1)$	$-Z/r_2+v_f(r_2)$	$(Z-3)$	$(Z-3)$
TPDW00	$-Z/r_1+v_i(r_1)$	$-Z/r_2+v_i(r_2)$	$(Z-4)$	$(Z-4)$

$$v_i(r_1) = 2\langle\varphi_{2s}(\mathbf{r}_2,\mathbf{r}_3)|\frac{1}{r_{12}}|\varphi_{2s}(\mathbf{r}_2,\mathbf{r}_3)\rangle + 2\langle\varphi_{1s}(\mathbf{r}_4,\mathbf{r}_5)|\frac{1}{r_{14}}|\varphi_{1s}(\mathbf{r}_4,\mathbf{r}_5)\rangle. \quad (20)$$

The final-state wave function $\Psi_f^{(-)}$ is approximated by the distorted wave $\phi_f^{(-)}$ in Eq. (14), where the wave functions $\chi_p^{(-)}(\mathbf{r}_1)$ and $\chi_s^{(-)}(\mathbf{r}_2)$ for the outgoing electrons are solved from the equations with distorting potentials U_p and U_s, respectively,

$$[c\alpha_1\cdot\mathbf{p}_1 + c^2\beta_1 + U_p - E_p]\chi_p^{(-)}(\mathbf{r}_1) = 0, \quad (21)$$

$$[c\alpha_2\cdot\mathbf{p}_2 + c^2\beta_2 + U_s - E_s]\chi_s^{(-)}(\mathbf{r}_2) = 0. \quad (22)$$

Various models of the distorting potentials U_p and U_s used in this work are summarized in Table I. In one extreme called model TPDW00, outgoing electrons completely screen each other such that they experience approximately the same distorting potential as the incoming electron. In the other extreme called model TPDW11, the mutual screening effects by outgoing electrons are completely ignored such that both the primary and secondary electrons are affected only by the nucleus and the bound electrons in the residual ion,

$$U_p = U_s = -\frac{Z}{r} + v_f(r), \quad (23)$$

where

$$v_f(r_1) = \langle\varphi'_{2s}(\mathbf{r}_2,\mathbf{r}_3)|\frac{1}{r_{12}}|\varphi'_{2s}(\mathbf{r}_2,\mathbf{r}_3)\rangle + 2\langle\varphi'_{1s}(\mathbf{r}_4,\mathbf{r}_5)|\frac{1}{r_{14}}|\varphi'_{1s}(\mathbf{r}_4,\mathbf{r}_5)\rangle. \quad (24)$$

In the more realistic model TPDW01, the faster primary electron is completely screened by the slower secondary electron in the asymptotic region such that the primary electron is affected by an asymptotic charge of $Z-4$ and the secondary electron by an asymptotic charge of $Z-3$. In the Be case, the primary and secondary electrons experience the screened potentials with asymptotic charges (0,0) in model TPDW00, (1,1) in model TPDW11, and (0,1) in model TPDW01.

III. RESULTS AND DISCUSSION

A. Total cross sections

For comparative studies of ionization cross sections of ions in an isoelectronic sequence, the threshold energy unit $u_i \equiv (E_i - c^2)/I$ is employed, where I denotes the ionization potential of the particular ion in consideration. Relativistic and nonrelativistic ionization potentials of selected Be-like ions are listed in Table II. We shall also use the reduced cross sections defined as

$$\sigma_R \equiv \left(\frac{I}{I_{Be}}\right)^2\sigma, \quad (25)$$

where I_{Be} denotes the ionization potential of the neutral Be atom.

The total cross sections for electron-impact ionization of Be-like ions in models TPDW00, TPDW01, and TPDW11 are calculated for incident energies from 1 to 10 threshold-energy units. Results for the neutral Be atom, which differ qualitatively from those of Be-like ions have been analyzed previously by Chang *et al.* [18] Results for target ions B^+, C^{2+}, N^{3+}, O^{4+}, Ne^{6+}, and Fe^{22+} are plotted in Fig. 1 along with available experimental and theoretical data for comparison. Cross sections in model TPDW00 are always smaller than those in models TPDW01 and TPDW11 near the threshold and larger for high incident energies. For small u_i, both continuum electrons share a small amount of kinetic energy

TABLE II. Ionization energies (in atomic units) of Be-like ions calculated in the Dirac-Fock method.

Ion	Ionization Energy (a.u.)	
	Relativistic	Nonrelativistic
B^+	0.861835	0.861593
C^{2+}	1.68319	1.68243
N^{3+}	2.75723	2.75547
O^{4+}	4.08320	4.07966
F^{5+}	5.66091	5.65456
Ne^{6+}	7.49049	7.47990
Al^{9+}	14.4935	14.4575
Ar^{14+}	31.2437	31.0890
Fe^{22+}	71.4641	70.7015
Ag^{43+}	192.752	185.717
Hg^{76+}	853.334	756.565

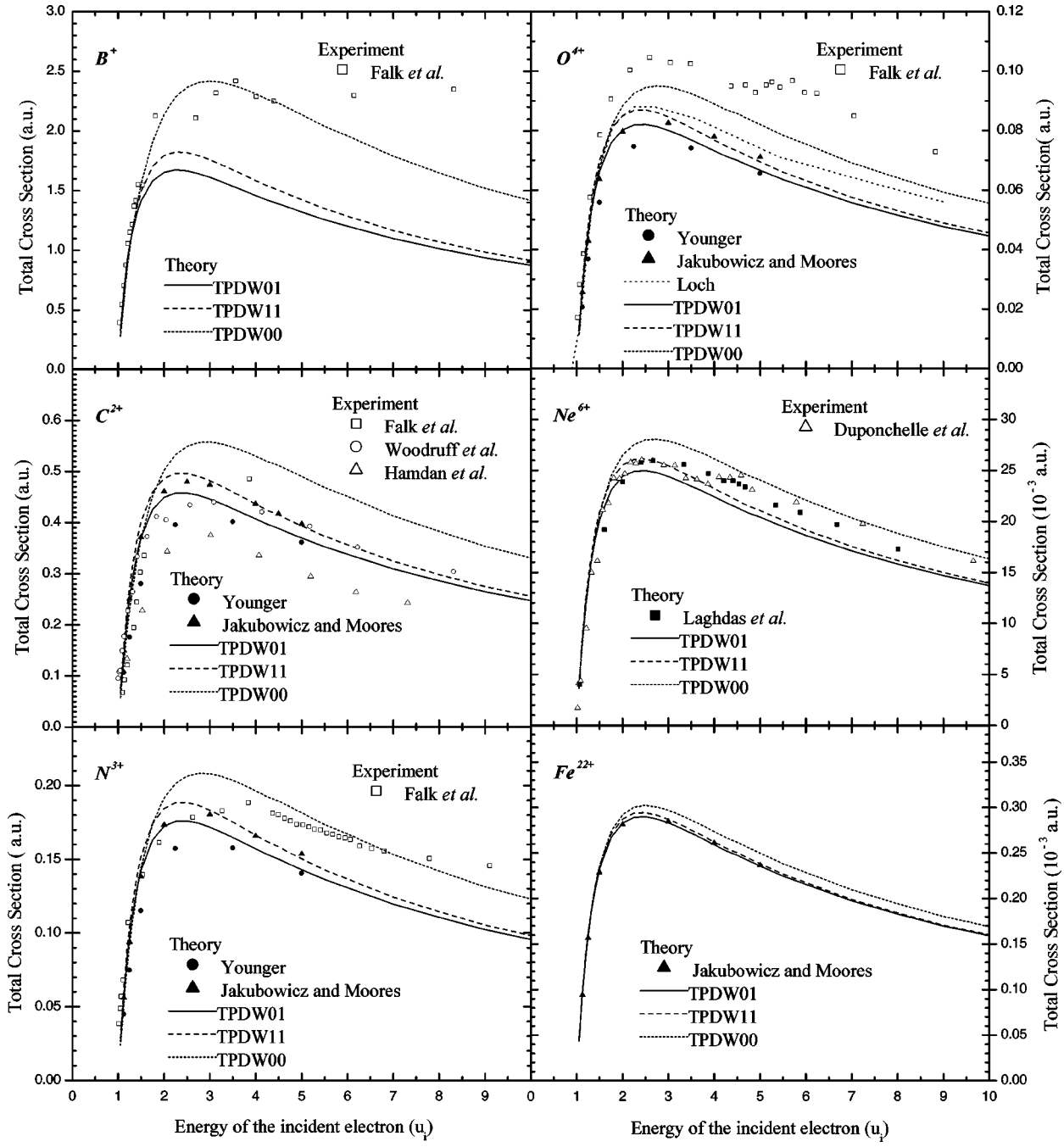

FIG. 1. Comparison of electron-impact ionization cross sections of B^+, C^{2+}, N^{3+}, O^{4+}, Ne^{6+}, and Fe^{22+}.

and move apart slowly. They spent much time near the nucleus and screen each other from the residual ion in a scenario which can be better described by model TPDW00. For large u_i, at least one of the continuum electrons carries large kinetic energy so that it flies away from the residual ion fast and produces little screening effects. Thus, either TPDW01 or TPDW11 will be more realistic. The differences between three models decrease as the atomic number Z of the target ion increases because the nuclear potential dominates the cross section for highly charged ions such that the mutual screening effects between continuum electrons in the final state do not affect the total cross section significantly.

In Fig. 1(a), we present the total cross sections of B^+ and compare with the experimental data of Falk *et al.* [1]. Our calculations are in fair agreement with experiment at low incident energies. At higher energies, the uncertainty of experiment is greater due to the assumption of constant background. In Fig. 1(b), our total cross sections of C^{2+} are compared with the experimental data by Falk *et al.* [1], by Woodruff *et al.* [2], and by Hamdan *et al.* [5], and the theoretical data by Younger [6] and by Jakubowicz and Moores [7]. It can be seen that our TPDW01 results in general agree quite well with others in all energy range. The experimental data by Hamdan *et al.* inhabit an uncertainty larger than 20%

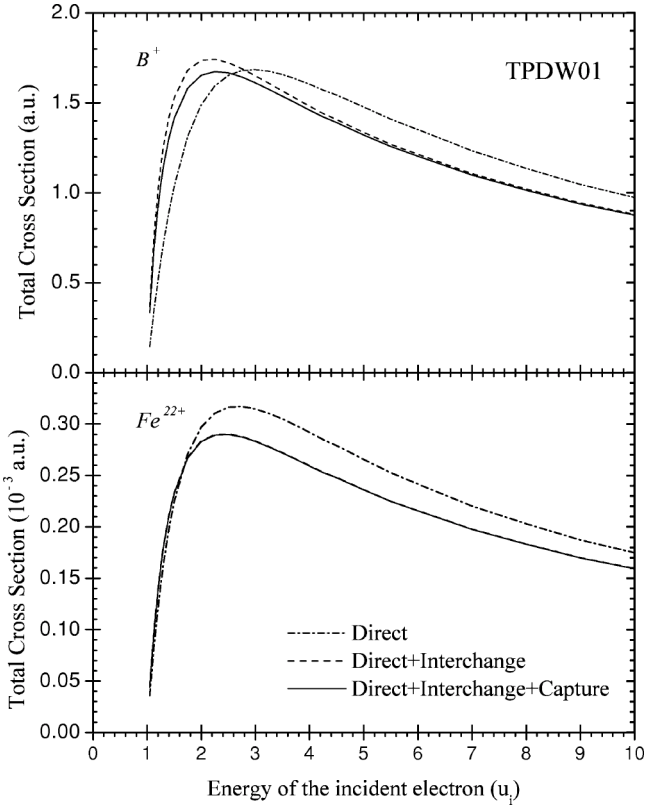

FIG. 2. Exchange effects on the ionization cross sections of B^+ and Fe^{22+} in model TPDW01.

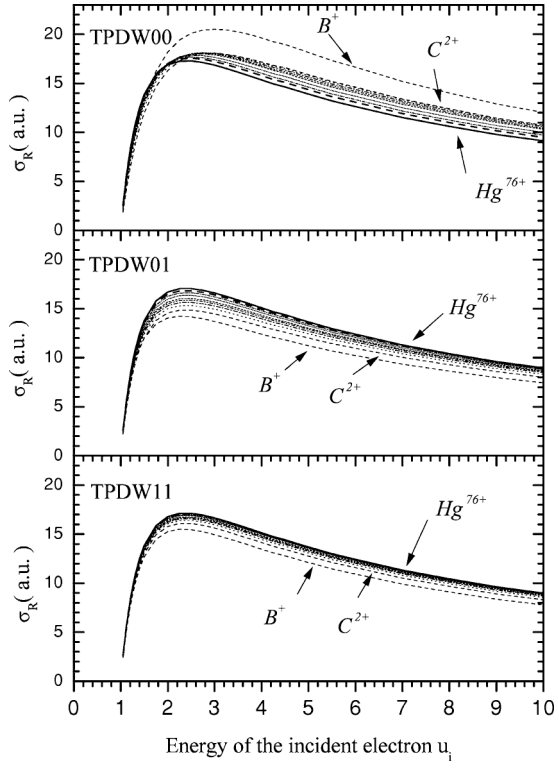

FIG. 3. Nonrelativistic reduced cross sections for B^+, C^{2+}, N^{3+}, O^{4+}, F^{5+}, Ne^{6+}, Al^{9+}, Ar^{13+}, Fe^{22+}, Ag^{43+}, and Hg^{76+} in models TPDW00, TPDW01, and TPDW11.

and appear to be smaller than all other data. In Fig. 1(c), we present the total cross sections of N^{3+} along with the experimental data by Falk *et al.* [1] and the theoretical data by Younger [6] and by Jakubowicz and Moores [7]. Our TPDW01 and TPDW11 results agree well with Jakubowicz and Moores' calculation. Falk's measurements are larger than all theoretical calculations at lower energies and approach our TPDW00 results at higher energies.

In Fig. 1(d), we present the total cross sections of O^{4+} and compare with the experimental data by Falk *et al.* [1] and the theoretical data by Younger [6], by Jakubowicz and Moores [7] and by Loch *et al.* [3]. All theoretical data are in fair agreement among themselves while Falk's measurements appear to be higher in all energy ranges. The ratio of metastable states is not estimated in the measurements by Falk *et al.* for N^{3+} and O^{4+}, which makes the results less reliable. In Fig. 1(e), the total cross sections of Ne^{6+} are compared with the experimental data by Duponchelle *et al.* [4] and the theoretical data by Laghdas *et al.* [8] Both the experimental and theoretical data are in fair agreement with our calculations. In Fig. 1(f), our total cross sections of Fe^{22+} are compared with the theoretical data by Jakubowicz and Moores [7]. With the increase of the nuclear charge, the electron-electron correlations become relatively insignificant, and all calculations more or less agree with each other.

B. Exchange effects

To analyze exchange effects in electron-impact ionization, total cross sections with direct terms, with direct plus interchange terms, and with direct plus interchange and capture terms are compared. It is found that exchange effects on the total cross section are relatively more complicated for low-*Z* ions. We present results of B^+ and Fe^{22+} in model TPDW01 as representatives of low- and high-*Z* ions in Fig. 2. We note that the effects of interchange terms in the transition amplitude raise the cross section near threshold and lower it as the excess energy increases. At low energies, the interchange terms increase the total cross section as much as three times for B^+ and increase by about 20% for Fe^{22+}, whereas, at high energies, the interchange terms decrease the total cross section by about 10% for all ions.

The effects of capture terms are important for low-*Z* ions, especially near threshold, and negligible for high-*Z* ions as shown in Fig. 2. This can be explained because the bound electrons spread out more for low-*Z* ions so that there is more chance for the incident electron to overlap and exchange roles with the bound electrons. For high-*Z* ions, on the other hand, the bound electrons are more tightly bound so that there is less chance to exchange energy with the incident electron.

C. Relativistic effects and scaling law

Nonrelativistic reduced cross sections for B^+, C^{2+}, N^{3+}, O^{4+}, F^{5+}, Ne^{6+}, Al^{9+}, Ar^{13+}, Fe^{22+}, Ag^{43+}, and Hg^{76+} in models TPDW00, TPDW01, and TPDW11 are presented in Fig. 3. It can be seen that cross-section curves approach a universal curve with increasing *Z*. The universal curve suffices to describe the nonrelativistic reduced cross sections in the

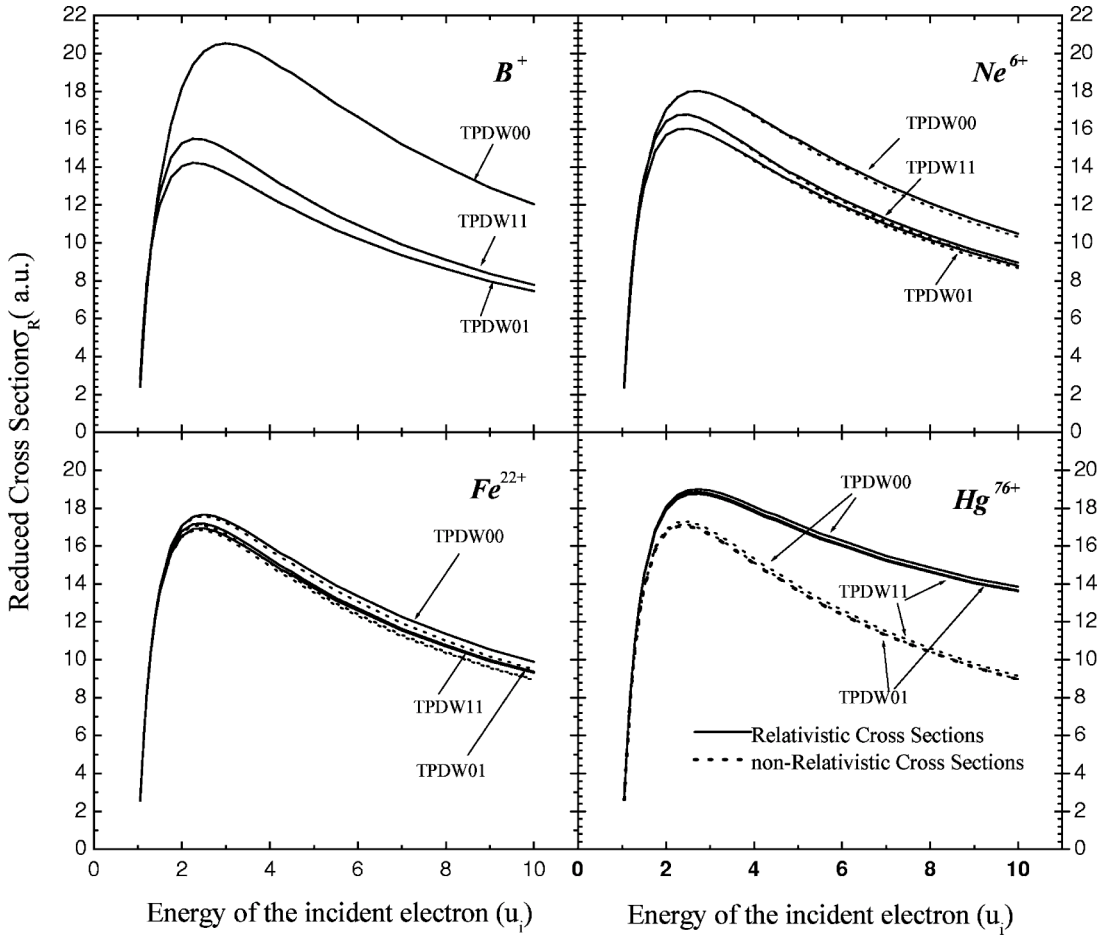

FIG. 4. Relativistic and nonrelativistic reduced cross sections for B^+, Ne^{6+}, Fe^{22+}, and Hg^{76+} are plotted in the solid lines and dotted lines, respectively.

high-Z limit. This asymptotic behavior of ionization cross sections provides an excellent tool to estimate cross sections for highly charged ions.

Nonrelativistic and relativistic reduced cross sections for B^+, Ne^{6+}, Fe^{22+}, and Hg^{74+} are plotted in dotted and solid lines, respectively, in Fig. 4. In the upper left panel for B^+, the three solid lines represent the relativistic reduced cross sections in models TPDW00, TPDW01, and TPDW11. The reduced cross sections in their nonrelativistic limits are very close to and indistinguishable from the corresponding relativistic results in each model. In the upper right panel for Ne^{6+}, the reduced cross sections from the three potential

TABLE III. Fitting parameters for electron impact ionization of Be-like ions under model TPDW01, where $\sigma_R = 1/u_i(1-1/u_i)(a_0 - a_1/u_i + a_2/u_i^2)$.

Ion	Nonrelativistic			Relativistic		
	a_0	a_1	a_2	a_0	a_1	a_2
B^+	97.14	163.77	151.78	97.16	164.04	152.14
C^{2+}	105.00	179.02	154.48	105.15	180.17	155.95
N^{3+}	108.97	186.60	160.80	109.09	187.14	161.18
O^{4+}	111.12	189.39	162.84	111.39	190.67	163.98
F^{5+}	112.39	189.99	162.63	112.73	191.42	163.80
Ne^{6+}	113.25	190.47	162.97	114.17	193.51	165.51
Al^{9+}	114.27	187.83	159.24	115.87	196.33	168.79
Ar^{14+}	114.92	185.13	155.58	118.06	200.60	172.49
Fe^{22+}	115.54	184.22	154.84	122.70	219.47	192.98
Ag^{43+}	115.60	183.57	153.98	142.69	309.18	290.62
Hg^{76+}	115.67	180.73	151.28	201.79	595.90	602.63

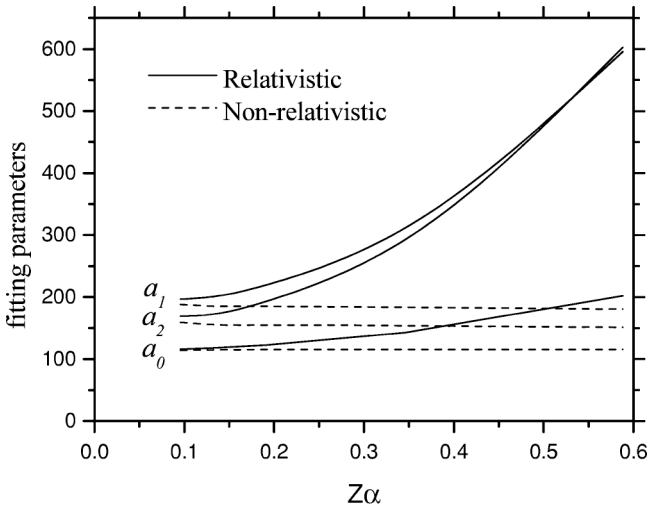

FIG. 5. The Z dependence of fitting parameters a_0, a_1, and a_2, where α is the fine-structure constant.

models get closer since the increasing of the nuclear charge makes the electron-electron correlations relatively unimportant, and the relativistic effects can barely be seen in the figure. In the lower left panel for Fe^{22+}, the solid lines get even closer to each other while the differences between relativistic and nonrelativistic results become noticeable at high incident energies. In the lower right panel for Hg^{74+}, in which the nuclear charge is substantially high, the differences between various potential models become negligibly small, while relativistic effects are significant at all incident energies.

A scaling law has been given in the Bethe-Born theory as $\sigma=(1/u_i)(A \ln u_i+B)$ where A and B are constants. Moores and Nussbaumer [19] have attempted to include the relativistic effects by using the Mott-Massey formula,

$$\sigma=\frac{A}{u_i}\left\{\ln u_i+B-\ln\left(1-\frac{v^2}{c^2}\right)-\frac{v^2}{c^2}\right\}, \tag{26}$$

where v is the velocity of the incident electron. In this formula, a relativistic form of the energies of incident electron is adopted. The parameter A may be determined from the photoionization cross section, and B by fitting to the Coulomb-Born results. Supposedly, both A and B depend on the nuclear charge Z; however, the Z dependence along isoelectronic sequences has not been discussed.

In this work, we propose to fit the reduced cross section σ_R by a relatively simple formula in powers of $1/u_i$ as

$$\sigma_R=\frac{1}{u_i}\left(1-\frac{1}{u_i}\right)\left(a_0-\frac{a_1}{u_i}+\frac{a_2}{u_i^2}\right). \tag{27}$$

Fitting parameters for selected ions are listed in Table III. The confidence of the fitting is better than 99.9%. It can be seen that the fitting parameters a_0, a_1, and a_2 vary slowly with the nuclear charge Z in the nonrelativistic limit, while they have a strong Z dependence with relativistic effects included.

TABLE IV. The Z dependence of fitting parameters a_0, a_1, and a_2 approximated by a second-degree polynomial of $Z\alpha$, e.g., $a_i=p_0+p_1(Z\alpha)+p_2(Z\alpha)^2$, where α is the fine-structure constant.

	p_0	p_1	p_2
a_0	115.11	−15.25	276.26
a_1	199.25	−172.94	1440.29
a_2	172.66	−199.96	1582.55

To study the Z dependence of the relativistic cross section, we plot the fitting parameters as functions of $Z\alpha$ in Fig. 5 for ions with $Z>10$, where α is the fine-structure constant. It is found that these parameters can be described quite well by second-degree polynomials of $Z\alpha$. The expansion coefficients are listed in Table IV. The confidence of the fitting is as good as 99.8%. With these expansion coefficients, we can predict the relativistic cross sections for any ion in the same isoelectronic sequence.

To further demonstrate relativistic effects for highly charged ions along the Be isoelectronic sequence, we scaled the reduced cross sections to $u_i\sigma_R$. The Z dependence of the scaled cross sections $u_i\sigma_R$ is presented in Fig. 6. We see that for a specific incident energy u_i the nonrelativistic scaled cross sections remain almost constant as Z increases beyond 10. For ions with Z lower than 10, where electron-electron correlations are relatively more important, this simple trend of cross sections becomes invalid. With relativistic effects included, the scaled cross section remains unchanged at the low-Z end but grows up rapidly as Z increases at high incident energies. For example, relativistic effects on the ionization cross section of a target ion with $Z<10$ is negligible for all incident energies. For targets with $Z\approx 20$, the relativistic effects will enhance the cross sections by about 2% for an incident electron with $u_i=5$ and 2.5% for $u_i=10$. For medium targets with $Z\approx 40$, the relativistic effects will increase the cross sections by about 8% for $u_i=5$ and 12% for $u_i=10$. For $Z\approx 60$, the cross sections increase by about 16% for $u_i=5$ and 28% for $u_i=10$; for $Z=80$, by 29% for $u_i=5$ and 50% for $u_i=10$.

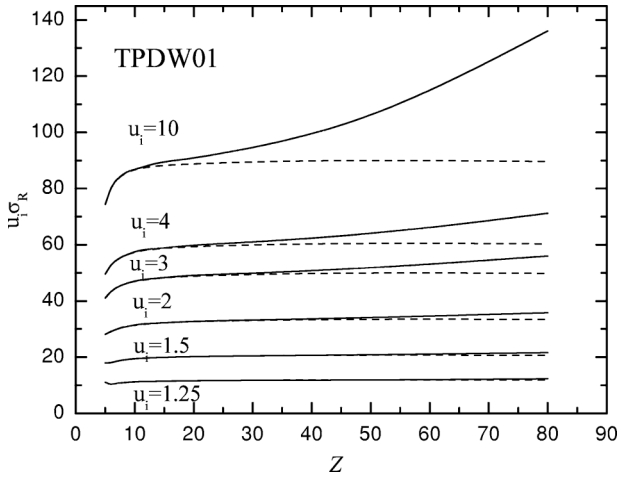

FIG. 6. The Z dependence of $u_i\sigma_R$ in model TPDW01. The solid and dashed lines are for relativistic and nonrelativistic cross sections, respectively.

IV. CONCLUSION

A fully relativistic calculation of the electron-impact ionization for Be-like ions is performed. Exchange effects are included by antisymmetrizing the transition amplitudes in the two-potential distorted-wave approximation. Three different sets of asymptotic charges are used for the distorting potential to study the mutual screening of the primary and secondary electrons. For small Z, the cross section is dominated by electron-electron correlations between the two final continuum electrons while relativistic effects are negligible. In this case, the capture processes are also important. We note here that the capture terms correspond to the exchange process of the direct ionization. It is nothing to do with two-step processes, such as ionization-autoionization, which may be also important in some cases. The cross sections arising from indirect processes should be investigated for further understanding of the electron-impact ionization processes. Exchange effects are separated into interchange and capture terms. The interchange terms modify the total cross section at all incident energies for all Z. The capture terms play an important role only near threshold. Relativistic effects are studied by comparison with the ionization cross section in the nonrelativistic limit, where the nonrelativistic ionization cross section can be described by a scaling law. The reduced cross section can be described very well by a polynomial function of $1/u_i$, the inverse of incident energy. The expansion coefficients are almost constant for nonrelativistic cross sections. Relativistic effects are significant for high-Z ions which give rise to a $Z\alpha$ dependence for the expansion coefficients. Cross sections for any ions of interest along the Be isoelectronic sequence can be easily derived by interpolating from the provided data.

[1] R. A. Falk, G. Stefani, R. Camilloni, and G. H. Dunn, Phys. Rev. A **28**, 91 (1983).

[2] P. R. Woodruff, M. C. Hublet, M. F. A. Harrison, and E. Brook, J. Phys. B **11**, L679 (1978).

[3] S. D. Loch, J. Colgan, M. S. Pindzola, M. Westermann, F. Scheuermann, K. Aichele, D. Hathiramani, and E. Salzborn, Phys. Rev. A **67**, 042714 (2003).

[4] M. Duponchelle, M. Khoulid, E. M. Oualim, H. Zhang, and P. Defrance, J. Phys. B **30**, 729 (1997).

[5] M. Hamdan, K. Birkinshaw, and J. B. Hasted, J. Phys. B **11**, L331 (1978).

[6] S. M. Younger, Phys. Rev. A **24**, 1278 (1981).

[7] H. Jakubowicz and D. L. Moores, J. Phys. B **14**, 3733 (1981).

[8] K. Laghdas, R. H. G. Reid, C. J. Joachain, and P. G. Burke, J. Phys. B **32**, 1439 (1999).

[9] H.-C. Kao, T.-Y. Kuo, H.-P. Yen, C.-M. Wei, and K.-N. Huang, Phys. Rev. A **45**, 4646 (1992).

[10] S.-W. Hsu, T.-Y. Kuo, C.-M. J. Chen, and K.-N. Huang, Phys. Rev. Lett. **A167**, 277 (1992).

[11] T.-Y. Kuo, C.-M. J. Chen, S.-W. Hsu, and K.-N. Huang, Phys. Rev. A **48**, 357 (1993).

[12] L. Sima, M. S. thesis, National Taiwan University, 1993 (unpublished).

[13] J.-C. Chang, C.-M. Wei, T.-Y. Kuo, and K.-N. Huang, J. Phys. B **27**, 4715 (1994).

[14] T.-Y. Kuo and K.-N. Huang, Phys. Rev. A **64**, 032710 (2001).

[15] J.-C. Chang and K.-N. Huang (unpublished).

[16] T.-Y. Kuo, H.-L. Sun, and K.-N. Huang, Phys. Rev. A **67**, 012705 (2003).

[17] K.-N. Huang, Phys. Rev. A **28**, 1869 (1983).

[18] J.-C. Chang, H.-L. Sun, W.-Y. Cheng, and K.-N. Huang (unpublished).

[19] D. L. Moores and H. Nussbaumer, J. Phys. B **3**, 161 (1970).